01 Jan 1973

Experiments on the Structure of Turbulence in Fully Developed Pipe Flow

T. R. Heidrick

S. Banerjee

R. S. Azad

EXPERIMENTS ON THE STRUCTURE OF TURBULENCE IN FULLY DEVELOPED PIPE FLOW

T. R. Heidrick and S. Banerjee
Atomic Energy of Canada Limited
Whiteshell Nuclear Research Establishment
Pinawa, Manitoba, Canada

R. S. Azad
Department of Mechanical Engineering
University of Manitoba
Winnipeg, Manitoba, Canada

ABSTRACT

This paper describes a series of two-point measurements in fully developed pipe flow. Measurements of the phase shifts between the Fourier components of the axial velocity fluctuations at two points were made with three different orientations of the two points. In all cases the two points were close enough together that the turbulent structure remained essentially "frozen" while passing between the sensors. The phase velocities, $C_1(f)$, and inclinations, $\alpha(f)$ (defined previously by Heidrick et al. (8)), of each frequency component, f, were determined from these measurements.

In general, the Fourier components are inclined to the wall - the lower frequencies making smaller angles with the wall than the higher frequencies. The higher frequency disturbances became more nearly perpendicular to the wall in the central region of the pipe. For points very near the wall the disturbances appear to be very obliquely inclined.

In the core region, the phase velocity increases with increasing frequency and there is little discernable trend in the phase velocities with respect to position when they are normalized by the local mean velocity. The group velocity of small scale disturbances (large wavenumbers) in the core region appears to be approximately constant and of the order of the local mean velocity. This means that a "frozen" pattern hypothesis should be valid for these scales.

All measurements became more scattered at values of $y^+ \lesssim 26$. This may be due to the intermittent nature of the flow near the wall since recent studies in turbulent shear flow suggest that energy transfer from the mean flow to fluctuations near the wall may be due to local instabilities ("bursts"). Thus, the time averaged model is not entirely adequate, and it was necessary to separate out the burst intervals for further study.

By suitably processing the two-point velocity signals it was possible to determine when the flow was bursting. The behavior of the velocity and vorticity within measured bursts was determined. This behavior and short-term energy spectra within bursts indicate a weakly periodic behavior. The overall behavior of the flow was shown to be similar to the last stage of the laminar-to-turbulent flow transition.

INTRODUCTION

The structure of turbulence near walls in boundary layers and conduits has been extensively investigated. The early studies of Prandtl (18) and von Karman (27) developed models of the turbulence structure that permitted calculation of the mean velocity field for various flow conditions and geometries. More recently, Townsend (24,26) tried to characterize the complex motions near the wall in terms of a few prevailing types of eddies.

Townsend shows how an assumed large scale structure will fit measured correlation function measurements. The reverse process of inferring a structure from a series of correlation functions is (as noted by Townsend) ambiguous since many different structures can give the same correlation. None-the-less, the space-time correlation measurements of various investigators (summarized up to 1964 by Favre (5)) have provided some insight into the types of motion that exist in turbulent shear flows.

The central difficulty in interpreting space-time correlations in shear flows arises because different eddy sizes may move at different speeds. Thus, the different Fourier components of the fluctuating velocity field may move past a measuring point at different velocities. The problem of interpretation is made even more difficult (as pointed out by Sternberg (23)) because the disturbances may be inclined to the wall; the degree of inclination being a function of the scale of the motion. The first objective of this work was to determine local convection velocities for the frequency components and the angle at which the disturbances are inclined to the wall in a turbulent pipe flow.

Instead of trying to calculate a dominant structure, Kline and co-workers (10, 12) visually observed the flow structure near the wall of a turbulent boundary layer. These studies showed that longitudinal 'streaks' of slow- and fast-moving fluid exist side by side near the wall of a turbulent boundary layer. Intermittently, the low speed streaks would

(i) lift away from the wall

(ii) develop into either transverse or streamwise vortices which migrated away from the wall,

(iii) eventually these vortices broke up into a more chaotic motion.

This three stage cycle was called "bursting" or an active period. The existence of intermittent periods of activity in the midst of relatively quiescent intervals suggests that a single "average" model may not describe the turbulent structure very near the wall. Thus, the second objective of this work was to study this intermittent character of the flow near the wall.

THEORETICAL BASIS FOR THE DETERMINATION OF CONVECTION VELOCITIES AND INCLINATIONS

The theoretical basis for determination of convection velocities and inclinations has been given previously by Heidrick et al. (6), Heidrick et al. (8), and Heidrick (9) and will be briefly reviewed here.

The cross spectral density between axial velocity fluctuations at two points 1 and 2, consists of a real part, the co-spectrum, Co(f), and an imaginary part, the quadrature, Q(f). A measure of the correlation between each frequency component is the coherence,

$$R(f) = \left| \frac{Co^2(f) + Q^2(f)}{G_1(f)\, G_2(f)} \right|^{1/2} \qquad (1)$$

where $G_1(f)$ and $G_2(f)$ are the one-dimensional spectra measured at points 1 and 2, respectively. For frequencies where this correlation is high the phase of the cross spectrum $\theta_{12}(f) = \tan^{-1}(Q(f)/Co(f))$ may be interpreted as the phase shift caused by the spectral component moving from point 1 to point 2 (see Reference 9). The spectral component may be thought of as "frozen" as it translates between the points. The spectral component is an abstraction in the same sense as an eddy based on average statistical properties of the flow. Each component can be thought of as having an individual size based in its frequency and speed. For the situation shown in Figure 1

$$\theta_{12}(f) = \frac{2\pi f r}{C_1(f)} \left| \sin\beta\cot\alpha(f) - \cos\beta \right| \qquad (2)$$

Measuring $\theta_{12}(f)$ with sensor configurations having two different values of β, such as any two of the three in Figure 2, solves this equation for the two unknowns, $C_1(f)$ and $\alpha(f)$. The measurements presented below were taken with the three orientations shown so that $\alpha(f)$ and $C_1(f)$ could be determined in three different ways and hence the results could be compared.

Even for a "frozen" pattern convecting past the two measuring points there will be a distribution of phase velocities associated with each frequency. An average phase velocity can be calculated by the above technique but no information is obtained about the distribution. This is not a serious drawback, however, since Morrison (17) has shown that the distribution of phase velocities is quite concentrated about the mean.

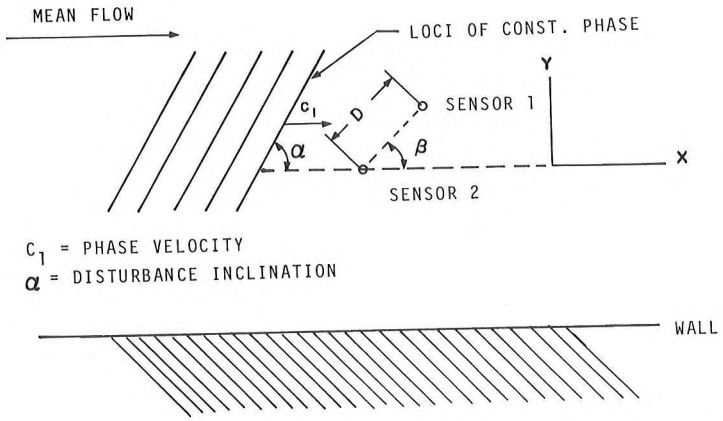

Figure 1. Schematic diagram of a disturbance in a "frozen" pattern in relation to the sensors and the wall.

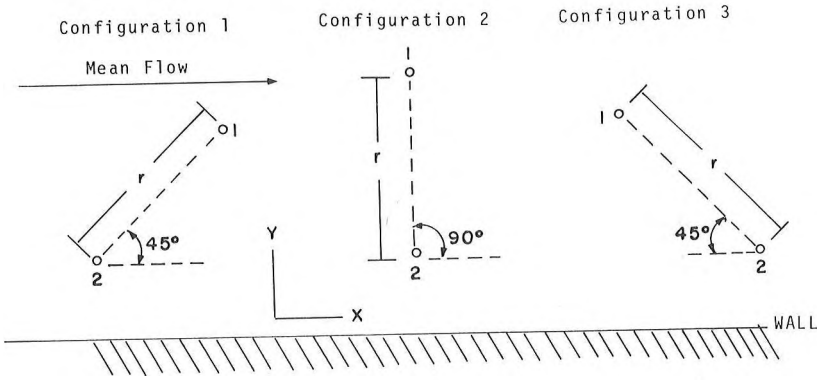

Figure 2. Configurations of the two sensor probes used in the study. All sensor diameters were 0.0508 mm. and r = 0.254 mm.

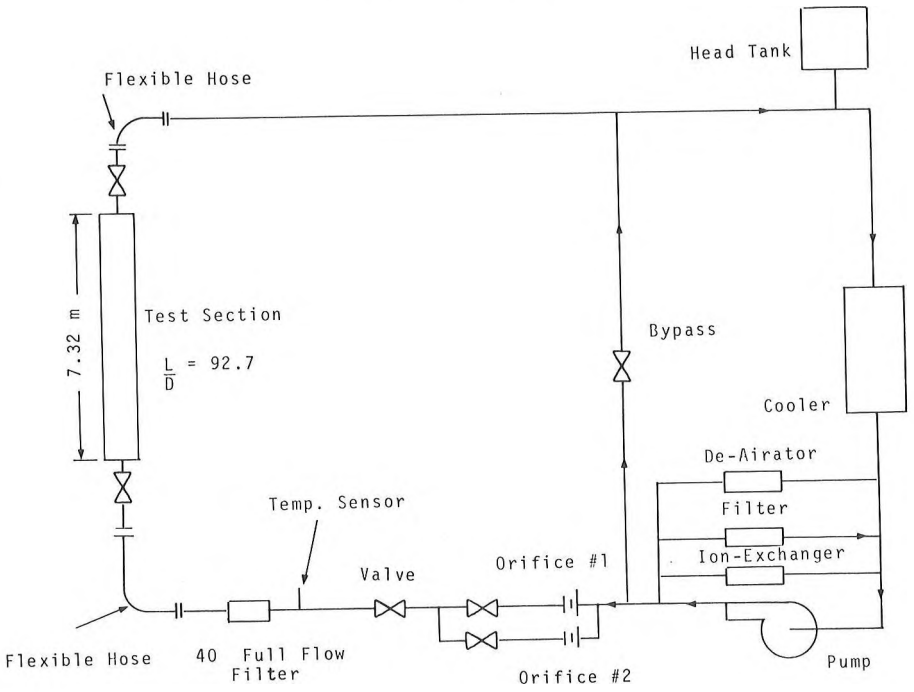

Figure 3. Schematic diagram of the experimental apparatus.

EXPERIMENTAL EQUIPMENT AND TEST FACILITY

Experimental Loop

The experiments were done in water (ν = 1.022 centistokes) in a 7.87 cm I.D. round tube inserted into the test apparatus shown schematically in Figure 3*. The inside surface of the last 1.21 meters of the test section were bored and polished. The ratio of the distance between the entrance and the measuring point to the inside diameter of the tube was 92.6. The water in the facility was maintained isothermal to within $\pm$0.05° by adjusting the cooling rate of the heat exchanger. The head tank was vented to atmosphere. Mean velocities were measured, and, as shown by Heidrick, et al. (8), were symmetric and best represented by Clauser's (3) equation in the log region. Turbulence intensities $\sqrt{\overline{u^2}}$ (8) agree with data taken in pipe flow by other investigators (such as Burchill (2)).

Velocity Sensors

The hot-film probes consisted of two T.S.I.+ 20 W sensors (0.051 mm dia. x 1.67 mm long, 1 mm heated length) placed 0.254 mm apart in the orientations shown in Figure 2. The sensor separation was from about 2 to 5 Kolmogoroff microscales (depending on the Reynold's number of the flow), if the dissipation is estimated from the mean flow variables. Thus the separation between the two sensors is of the order of the smallest length scales of significance.

The frequency response of the sensors was measured by the square wave test and matched and checked by raising the velocities high enough for eddy shedding. The vortex shedding frequency was the same for both sensors and in agreement with Roshko's measurements (19).

Anemometers, Signal Conditioning and Data Acquisition

The hot-film sensors were calibrated in the measuring section with a Pitot-static tube. Signals from the T.S.I. 1050 anemometers were linearized with DISA 55D10 linearizers. A D.C. voltage estimated to be near the mean was subtracted from the signals which were then low-pass filtered and amplified before being recorded on a Hewlett Packard 3914 analog tape recorder. The electronic and recording circuits for each channel were identical, but their characteristics were checked using sine wave inputs and a differential phase meter.

Digital Data Acquisition

The analog magnetic tape was played to an analog-to-digital (A-D) conversion facility described by Saltvold, et al. (20). The data were continuously stored on digital magnetic tape by removing them from the computer's memory faster than they were fed in by the A-D converter. Sampling rates of either 1000 or 2000 samples/sec for each A-D converter channel were used for either one- or two-minute records. The data were then processed using the fast Fourier transform algorithm of Cooley and Tukey (4). The spectra and statistical tests described by Heidrick (9) showed that both the sampling rates and record lengths were more than adequate.

RESULTS

Phase Velocities and Angles of Inclination

The phases of the cross spectra, $\theta_{12}(f)$, were measured at various positions with the three orientations shown in Figure 2. The time delays associated with phase shift,

$$\Delta t_{12}(f) = \frac{\theta_{12}(f)}{2\pi f} \tag{3}$$

were then calculated. A typical example, obtained during the Re_c = 15,600 experiments, is shown in Figure 4. The phases of the cross spectra (and hence the time delays) are subject to random error since they are estimated from finite record lengths. If the signals were Gaussian then the probability, p, that the true phase will lie in the interval $\theta_{12}(f) \pm \Delta\theta_{12}(f)$ is given by Stegen and Van Atta (22) as,

$$\sin^2\Delta\phi = \frac{1-R^2}{R^2}\left[(1-p)^{-2/DF} - 1\right] \tag{4}$$

where DF is the number of degrees of freedom of the estimate. The value of DF is twice the number of realizations for the 'fast Fourier transform' algorithm used in this study. R^2 is the true squared coherence but must be replaced by the measured squared coherence in this case. For the low frequency data obtained in this study the coherence is relatively constant at low frequencies and the phase decreases towards $\theta_{12}(f) = 0$. Hence, there is a frequency

*A more detailed description of the experimental arrangement and test section is given by Heidrick (9).

+Thermo Systems Inc.

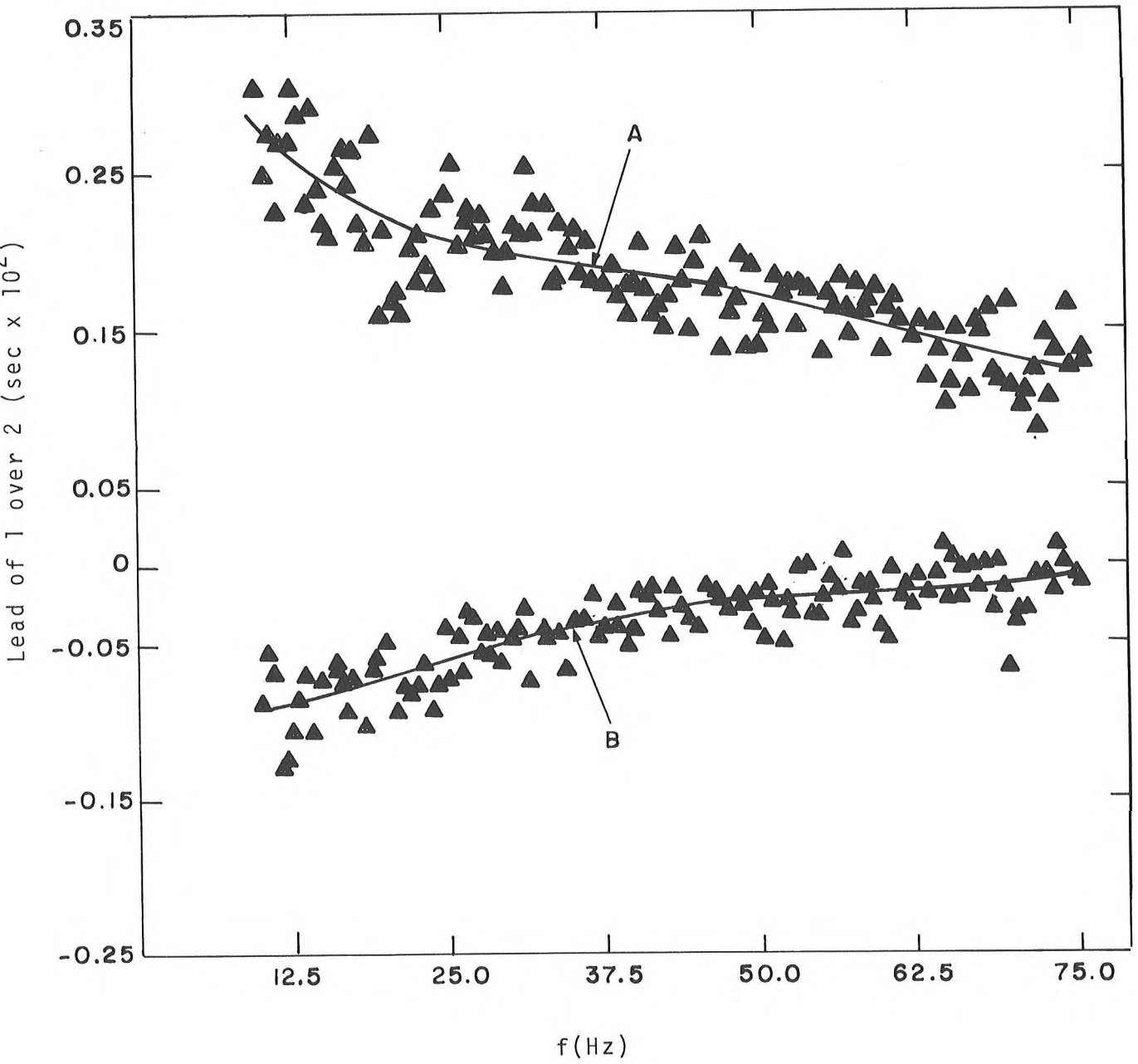

Figure 4. Typical time delay data from a probe of Configuration 1 when Re_c = 15,600. A - y_2^+ = 3.87, B - y_2^+ = 26.63. The variance in the data is due to the narrow analysis bandwidth used to ensure an unbiased estimate of the time delay (see Heidrick (9)).

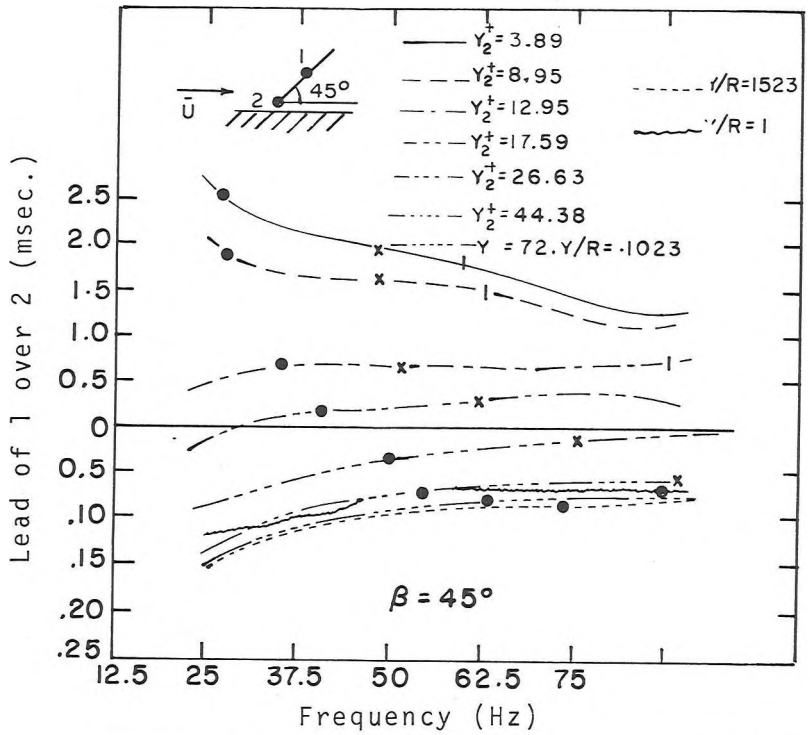

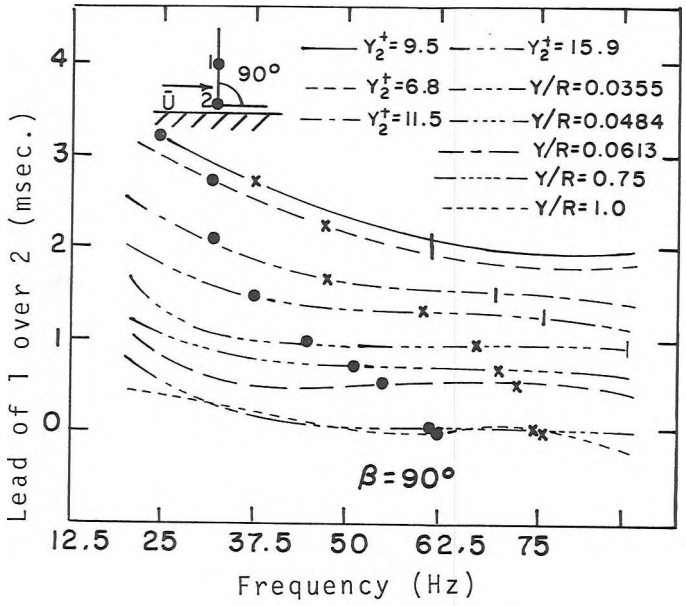

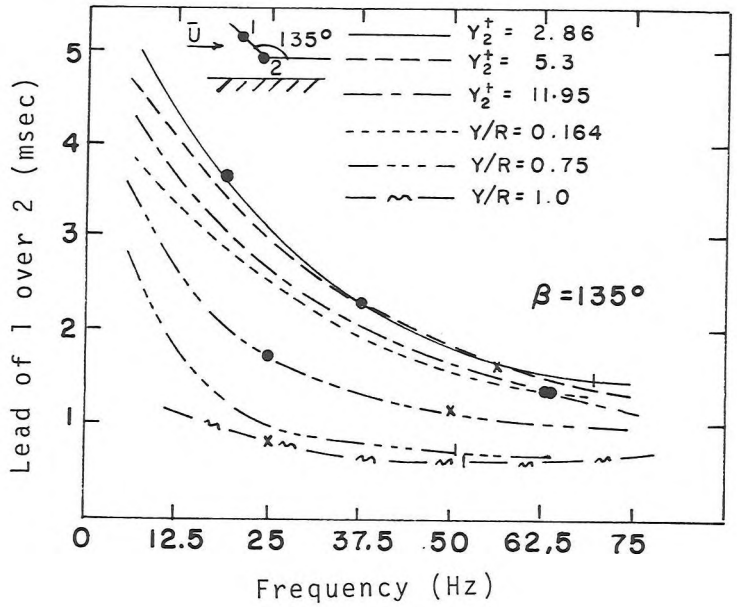

Figure 5. Time delay results measured with various probes when Re_c = 15,600. The ● indicates the frequency at which the squared coherence is 0.9 at which position. The x indicates a squared coherence of 0.8 and the ı 0.7.

below which $\theta_{12}(f)$ and $\Delta\theta_{12}(f)$ are comparable. This frequency is a lower bound on the range of frequencies where one can have confidence in the measurements of $\theta_{12}(f)$ or $\Delta t_{12}(f)$. The number of degrees of freedom used for all the low frequency results was 126. For R^2 of 0.95 and 0.90 this yields 95% confidence limits on the measured phase of 2.9 and 4.2 degrees, respectively.

Results for Re_c = 15,600

Since the data from each probe configuration were not taken at identical positions it was necessary to interpolate between the time delay results at different y-values. Each set of data was least squares fitted for this purpose by a polynomial. For example, the lines shown in Figure 4 are fits to the data shown. Figure 5 summarizes the time delays measured when Re_c = 15,600. Also indicated on these curves are several values of the coherence. The coherence appears to be higher at points closest to the center of the pipe.

Time delays were taken from Figure 5, interpolated to identical y-values, and then converted to the phase velocities and angles of inclination defined by Equation 2. Figures 6 and 7 show the phase velocities calculated in this manner using various sensor combinations. If the time delay measurements were perfect, then the values of $C_1(f)$ calculated with each pair of configurations would be identical. However, it is apparent that the results do not totally agree. Agreement between the results calculated from different sensor pairs is fairly good for $y/R \gtrsim .06$. However, the agreement closer to the wall (where the general coherence level is lower) is not good. If flow near the wall is made up of intermittent intervals of quasi-periodic behaviour interspersed in background turbulence (a possibility suggested in the next section) then a single time average wave model might not be expected to describe this near wall region.

Since each measurement of the time delay is prone to some amount of error, a 'best estimate' of $C_1(f)$ and $\alpha(f)$ can be chosen to minimize the total error in the measured time delays. A computer program was run on each data set to select the values of $C_1(f)$ and $\alpha(f)$ that minimized the least squares deviation of the measured time delays from the best values for the "time delays". These results are also indicated in Figures 6 and 7. The disagreement between sensors is now quantified by the standard error bars shown on alternate data points (except where noted). Figure 8 compares the 'best estimates' of $C_1(f)$ normalized by the local mean velocity at various central positions in the pipe. There is no discernible trend with respect to y/R, and all of the data fall within the band shown.

Figure 9 summarizes the best estimates of the angles of inclination ($\alpha(f)$ of Figure 2) of the frequency components at various positions. The components are more oblique to the wall ($\sim 72°$ at y/R = 0.063) at the closer positions to the wall. The angles approach 90° as the center of the pipe is approached. In general, the lower frequencies are more inclined to the wall. The points for each position appear to be merging as the frequencies become lower, and hence the scales become larger. If the large structures, which perhaps extend across all the positions shown, have a dominant angle then the points would all merge to form a single curve at low values of f. However, for structures of this type the values of $C_1(f)$ would also become independent of position at low frequencies. This does not appear to be the case. The measured phase delays for $f \lesssim 10$Hz are of the order of the statistical error involved in their measurement and hence cannot be used to draw any firm conclusions.

Figure 10 shows the data plotted in the form of radial frequency, ω, vs. wave number, $k = \omega/C_1(f)$. This plot permits the determination of a "group velocity". It is generally difficult (1) to physically define a "group velocity", Ug, except in simple circumstances. Fortunately, it is quite simple to define mathematically. The definition arises by considering two waves, A cos $(\omega_1 t - k_1 x)$ and A cos $(\omega_2 t - k_2 x)$, which are superimposed to give

$$\psi = A \cos(\omega_1 t - k_1 x) + A \cos(\omega_2 t - k_2 x) \quad (5)$$

If the waves have quite similar characteristics, i.e.,

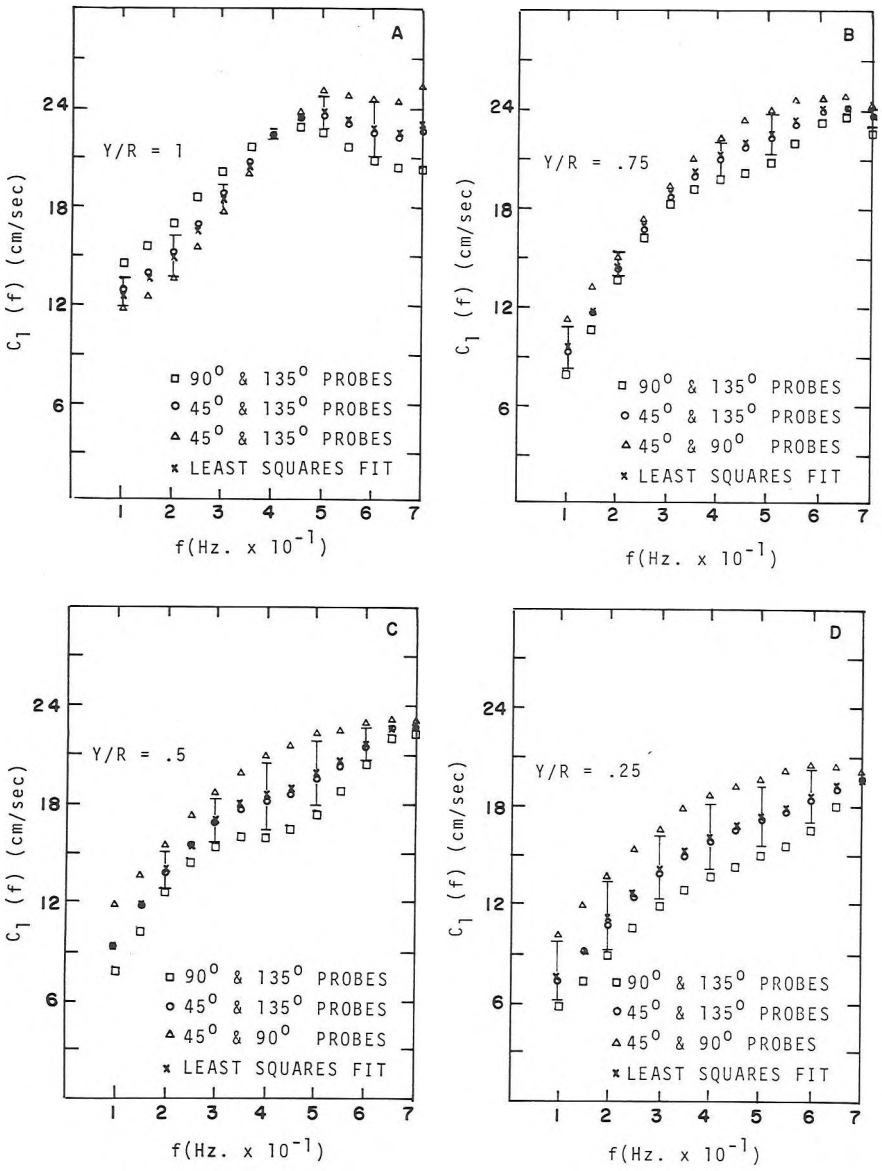

Figure 6. Phase velocities for $0.25 < Y/R < 1.0$ when Re_c = 15,600. The different symbols indicate the sensor combinations used to solve Equation 2.

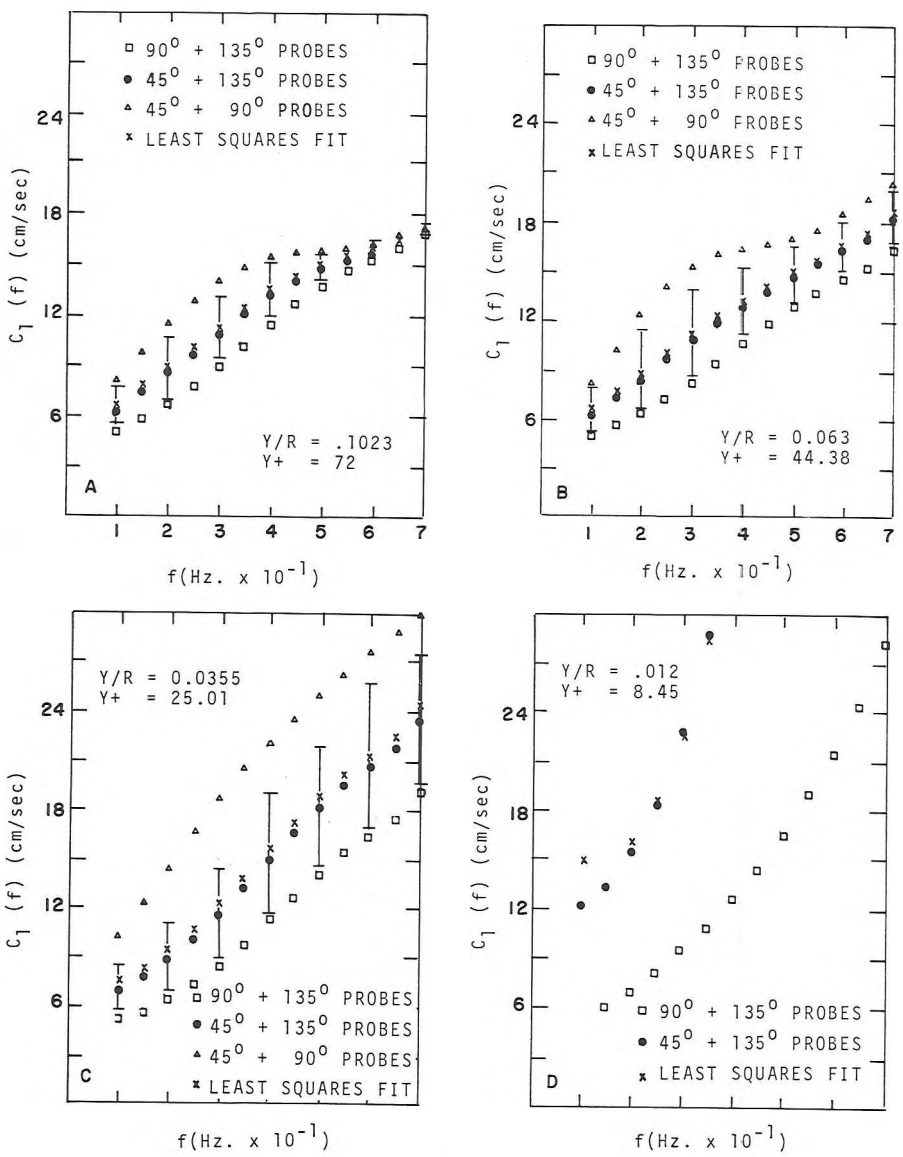

Figure 7. Phase velocities for $0.012 < Y/R < 0.102$ when Re_c = 15,600 symbols as in Figure 6.

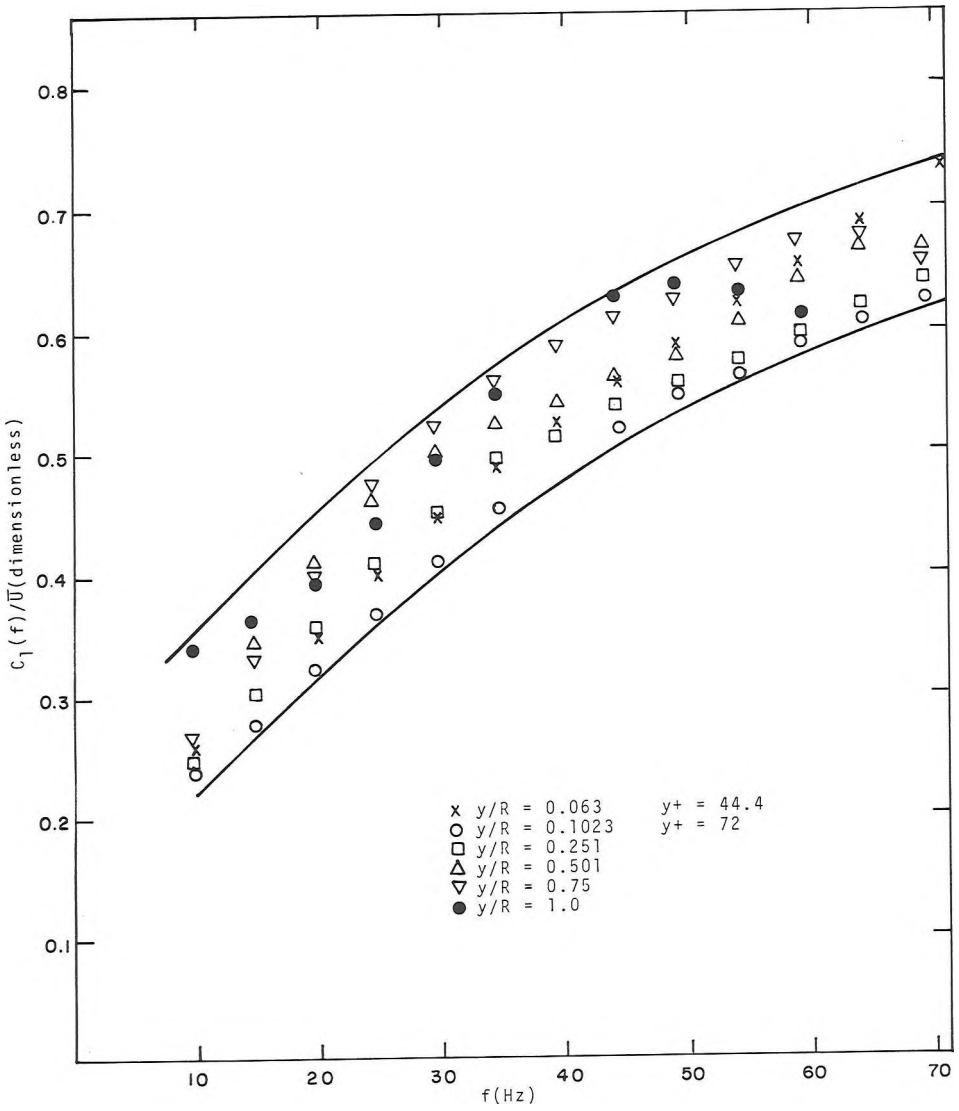

Figure 8. Phase velocities normalized by the local mean velocity at various positions in the core region of fully developed pipe flow at Reynold's number of 15,600.

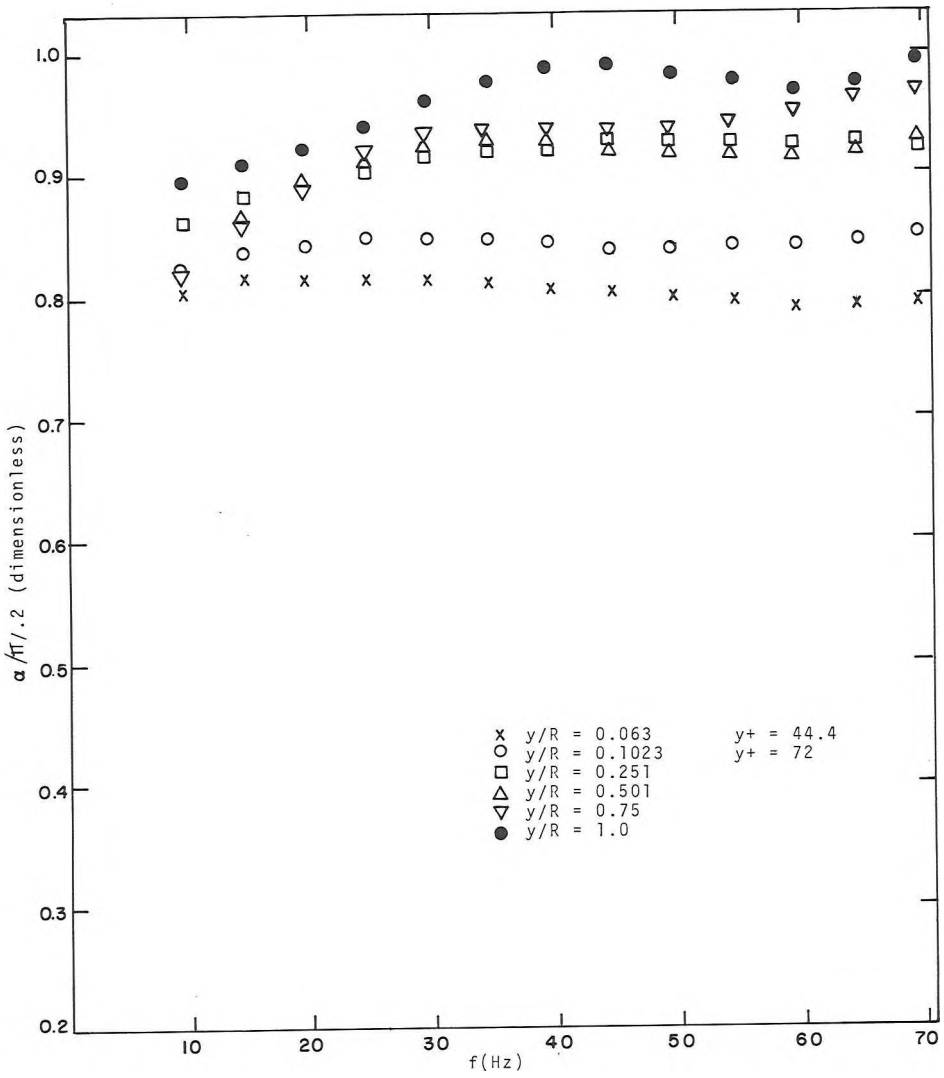

Figure 9. Angles of inclination (normalized by $\pi/2$) of the frequency components of u in the core region of fully developed pipe flow at a Reynold's number of 15,600.

$\omega_1 = \omega + \Delta\omega$ $\quad k_1 = k + \Delta k$

$\omega_2 = \omega - \Delta\omega$ $\quad k_2 = k - \Delta k$

then Equation 5 becomes

$$\psi = 2A \cos(\Delta\omega t - \Delta k x) \cos(\omega t - kx) \quad (6)$$

This is a carrier with frequency ω_1 and a modulation with frequency $\Delta\omega$. Thus, the wave may be described as a series of moving beats (or groups or wave-packets). The phase velocity is the velocity of the carrier, or

$$C = \frac{\omega}{k} \quad (7)$$

The group velocity is the velocity of the wave packets

$$Ug = \frac{\Delta\omega}{\Delta k} \text{ which } \rightarrow \frac{\partial\omega}{\partial k} \quad (8)$$

$$\text{as } \Delta k \rightarrow 0$$

Thus, mathematically $Ug = \frac{\partial\omega}{\partial k}$, and is physically the velocity of the wave packets formed by the superposition of the individual waves. When the data are plotted as $\omega = f(k)$, the phase velocity, $C_1(\omega)$, is the slope of the straight line joining the origin to any point on the curve at a frequency ω (i.e. Equation 7). The group velocity at ω is the slope of the tangent to the curve at ω (i.e. Equation 8).

At the higher wave number the group velocity is constant and equal to the local mean velocity at (y/R) positions of 0.1023 and 0.25. The scatter of the data becomes larger as the center of the pipe is approached, and it is difficult to determine if $Ug = \overline{U}$. However, the slopes of the curves are increasing (as they would if $\overline{U} = Ug$) and it appears certain that $Ug \sim \overline{U}$ for $k \gtrsim 250$ cm^{-1} at all positions in the core region of the pipe. The slopes of the best straight line fits to this region of k for $y/R \gtrsim 0.5$ are actually somewhat less than $\overline{U}$ for each case.

For situations (such as these higher wave numbers) where ω and k are linearly related, it can be shown (1) that the modulations or groups propagate at their velocity, Ug, without distortion. Thus, since the k'th wavenumber component of u is the recombination of several wavenumber components (i.e. the "group") the above is actually a modified frozen pattern approximation, i.e. the smaller scales ($k \gtrsim 250$ cm^{-1}) in the central region ($y/R \gtrsim 0.1$) of fully developed pipe flow at $Re_c = 15{,}600$ may be considered to be convecting in a frozen pattern at a constant velocity Ug very close to the local mean velocity.

Results for Re_c = 33,000 and 63,900

A similar analysis was also done at a Reynolds number of 33,000 and 63,900 over a more restricted range of y/R values. Phase velocities and angles of inclination are given by Heidrick (9) and in general show the same trends as for the Re=15,600 case.

The wave number vs frequency plot of the $Re_c = 33{,}000$ data (Figure 11) has more peculiarities at low wave numbers than the similar results at Re = 15,600. However, it again appears that the higher wave numbers have a constant group velocity of the order of the local mean. The line shown represents the mean velocity at y/R = 0.0378.

The group velocities measured when $Re_c = 63{,}900$ are shown in Figure 12. The slopes of the roughly linear portion of the data range from slightly greater than the local mean at y/R = 0.0097 to somewhat less than the local mean at y/R = .049 but are again constant over an appreciable range of wave numbers. Also becoming noticeable is a cut-off at high wave numbers. A cut-off of this sort is physically necessary since there is a finite lower limit to the size of the eddies in the turbulent stream. The physical dimension corresponding to the cut-off wave number ranges from 0.0014" to 0.00095".

Summary Remarks Regarding Phase Velocities and Angles of Inclination

The model proposed above was quite successful in depicting the small-scale characteristics of the axial velocity fluctuations in the region $y^+ \gtrsim 26$ of turbulent pipe flow. For all the Reynolds numbers investigated the large wavenumbers have constant

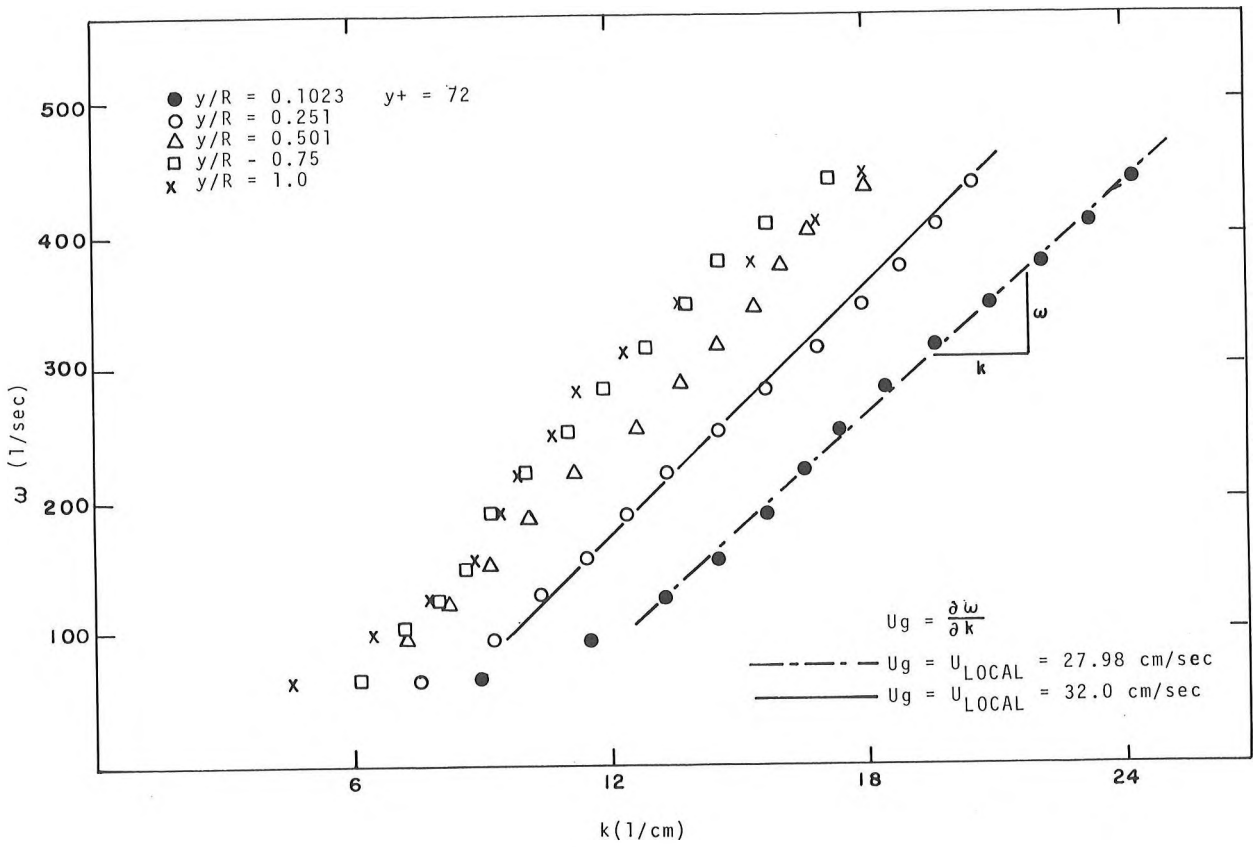

Figure 10. Radial frequency, ω, vs. wavenumber, k, at various positions when Re_c = 15,600.

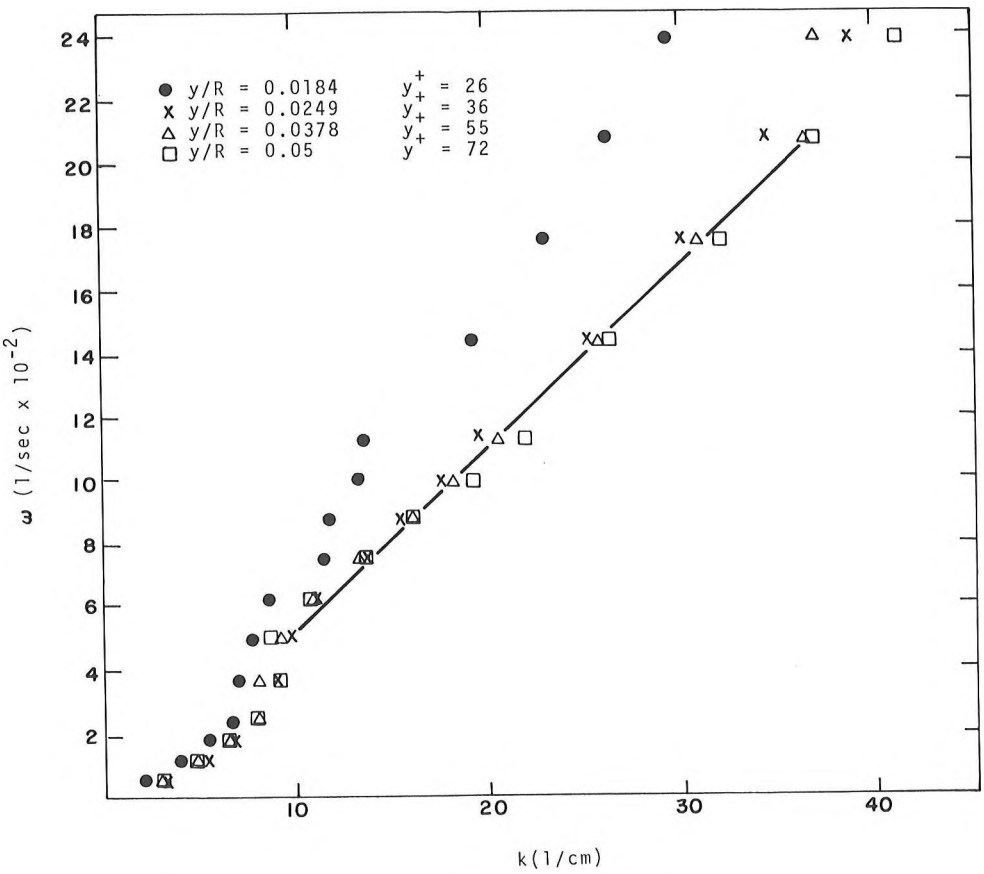

Figure 11. Radial frequency, ω, vs. wavenumber, k, at various positons when Re_c = 33,000.

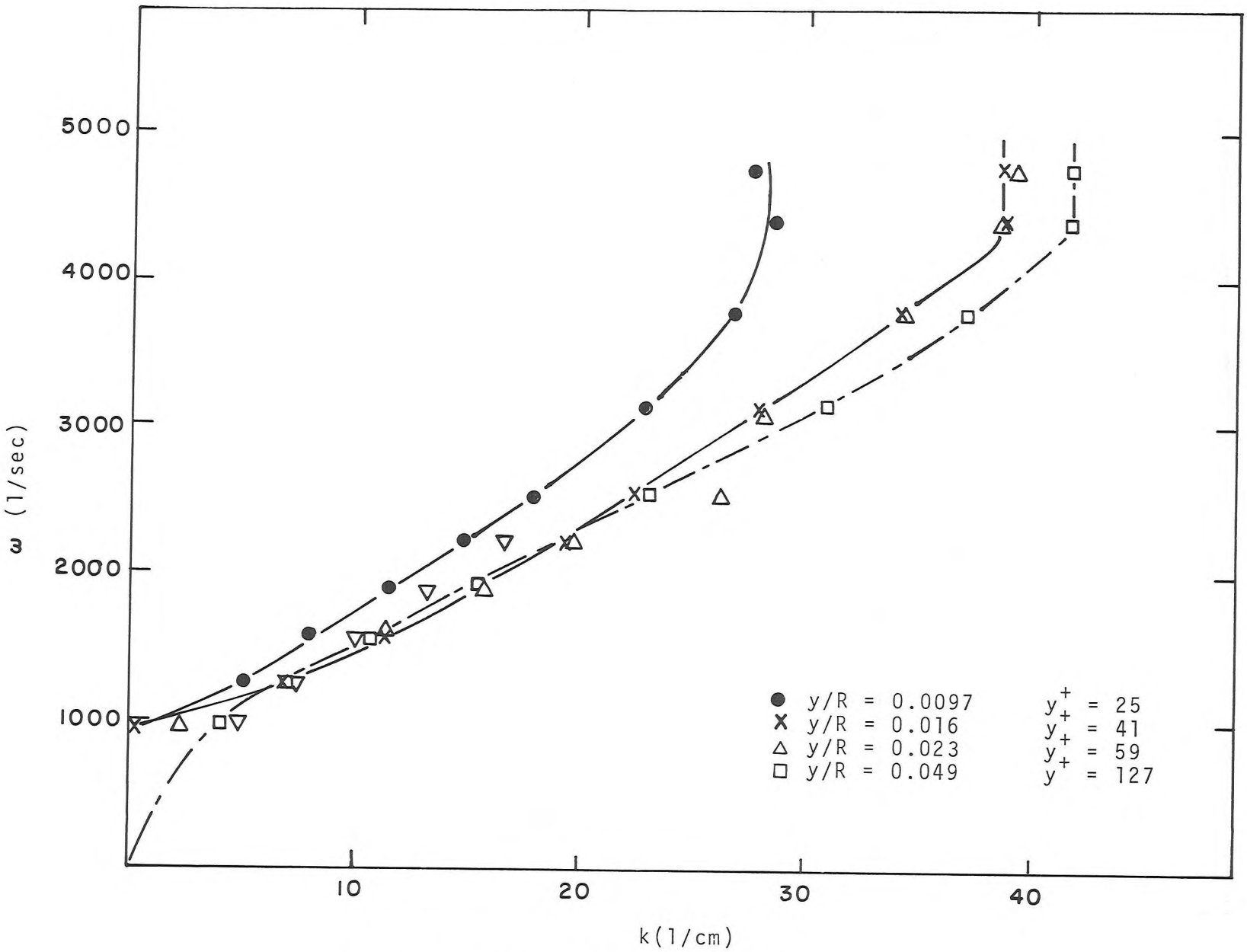

Figure 12. Radial frequency, ω, vs. wavenumber, k, for various positions in turbulent pipe flow when Re_c = 63,000.

group velocities of the order (within experimental error) of the local mean velocity.

In general the inclination of the frequency components is oblique to the wall at small y/R values, and becomes more perpendicular as the center of the pipe is approached. The lower frequencies are more inclined than the higher frequencies.

The model was, however, unsuccessful in the region $0 \lesssim y^+ \lesssim 26$ where the inclinations were very steep (i.e. $\alpha \lesssim 45°$ as indicated by Figure 4). Recent visual studies have shown that the near wall region consists of two distinct types of motion; (a) a quasi-periodic motion and (b) a more random type of background turbulence. The statistical behaviour of u(t) during motion type (a) may be completely different than during motion type (b). An average statistic over both types of intervals may be misleading. Thus, the work of the following section was undertaken to provide insight into how the intermittent intervals of quasi-periodic activity in the wall region affect the structure of the region near the wall.

Intermittent Character of the Near-Wall Region

The preceding discussion has shown that the character of flow near the wall may not be amenable to characterization by a single average model. It was, therefore, decided to study the intermittent character of this region, particularly the "bursts" described in the Introduction. Since the character of this region may be dominated by these active periods it was necessary to pick them out from the background and study their effect on the flow structure near the wall. The method developed to pick out the bursts from hot-film anemometer signals has been presented previously by Heidrick, et al. (8) and Heidrick (9). These references show that periods of activity in a filtered spatial velocity difference signal from probe configuration 1 of Figure 2 correspond to the bursts observed in the visual studies of Kim,et al. (10).

Figure 13 shows two cases of simultaneous values for u_1, $\frac{\partial u_1}{\partial t}$, $\frac{\partial u}{\partial r}$, and the envelope formed by the frequency component of our method of burst identification, for the conditions indicated. The beginning of an active period in the burst envelope is always accompanied by a positive spike in $\frac{\partial u}{\partial t}$. This is a necessary, rather than a sufficient, condition since an active period does not follow all peaks in $\frac{\partial u}{\partial t}$. The instant when u(t) is a relative minimum just before this spike is a convenient time to define as the beginning of an active period. Near the end of each active interval there is always a time when $\frac{\partial u}{\partial t} = 0$ which we define as its end. If the motion of the disturbance was pure translation the period between the beginning and end would correspond to its size in space.

If the flow consists of discrete pockets of activity (of the above size) distributed more or less randomly in space, then Figure 14 shows the behaviour of several variables within several of these bursts. The initial values of all variables have been subtracted (as shown in the title) since these represent the conditions measured in the flow just before the active pocket struck our probe. The vorticity has been calculated assuming a frozen pattern. With this reservation the abscissa of Figure 14 can be considered to be equivalent to the axial direction with the downstream direction being towards the left.

Each burst began with a relative minimum in u followed by simultaneous peaks in $\frac{\partial u}{\partial r}$, $\frac{\partial u}{\partial t}$, and ω_z. About half-way through the burst the vorticity peaked again, slightly after another relative minimum in axial velocity. The velocity minimums at the beginning of the burst and preceding the second vorticity peak were not sharp enough to be considered 'spikes' like those seen in the laminar-turbulent flow transition. However, the sequence of events is remarkably similar to the last stage of the breakdown of laminar flow to turbulent spots. Comparison of Figure 14 and the transition data of Kovasznay et al. (13) suggests the same mechanism is at work in both cases.

Kovasznay, et al. imposed a small 97 Hz fluctuation (which was also sinusoidal in the spanwise direction) on a laminar boundary layer and sensed its development with a ladder array of hot-wires. The distrubance was first amplified by the flow while retaining a roughly sinusoidal form. A negative spike then appeared in the axial velocity trace which was caused by low velocity fluid extending outward from the wall. In the last stage of

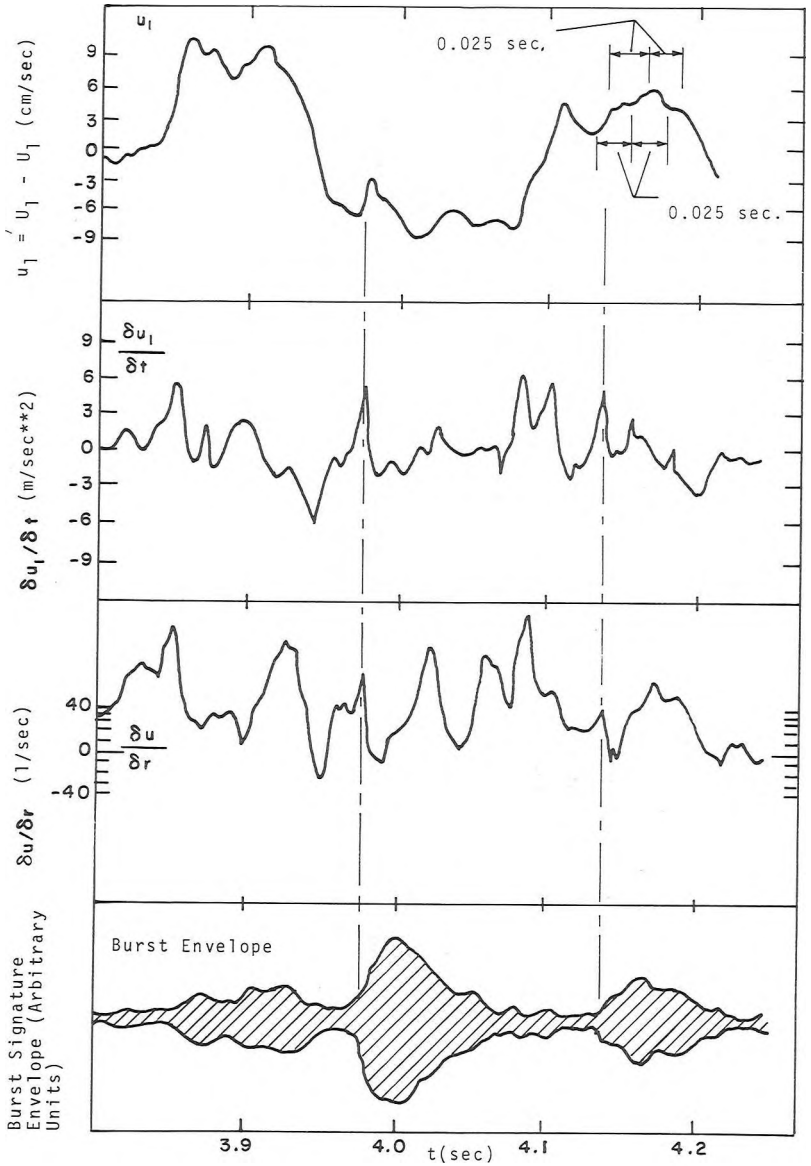

Figure 13a. Typical simultaneous velocity, time and space derivatives of velocity, and burst envelope from a probe of Configuration 1. Re_c = 15,600, y_2^+ = 12.96.

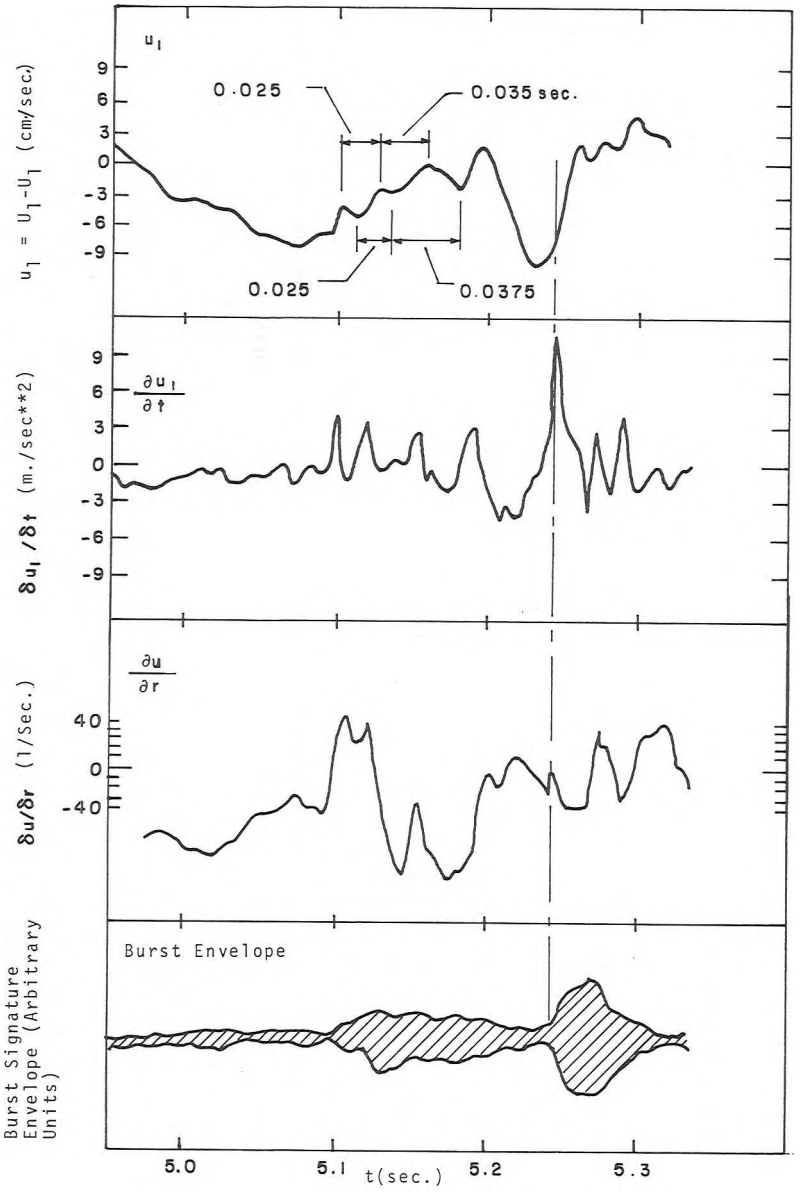

Figure 13b. Same as Figure 13a, but over a different interval of time.

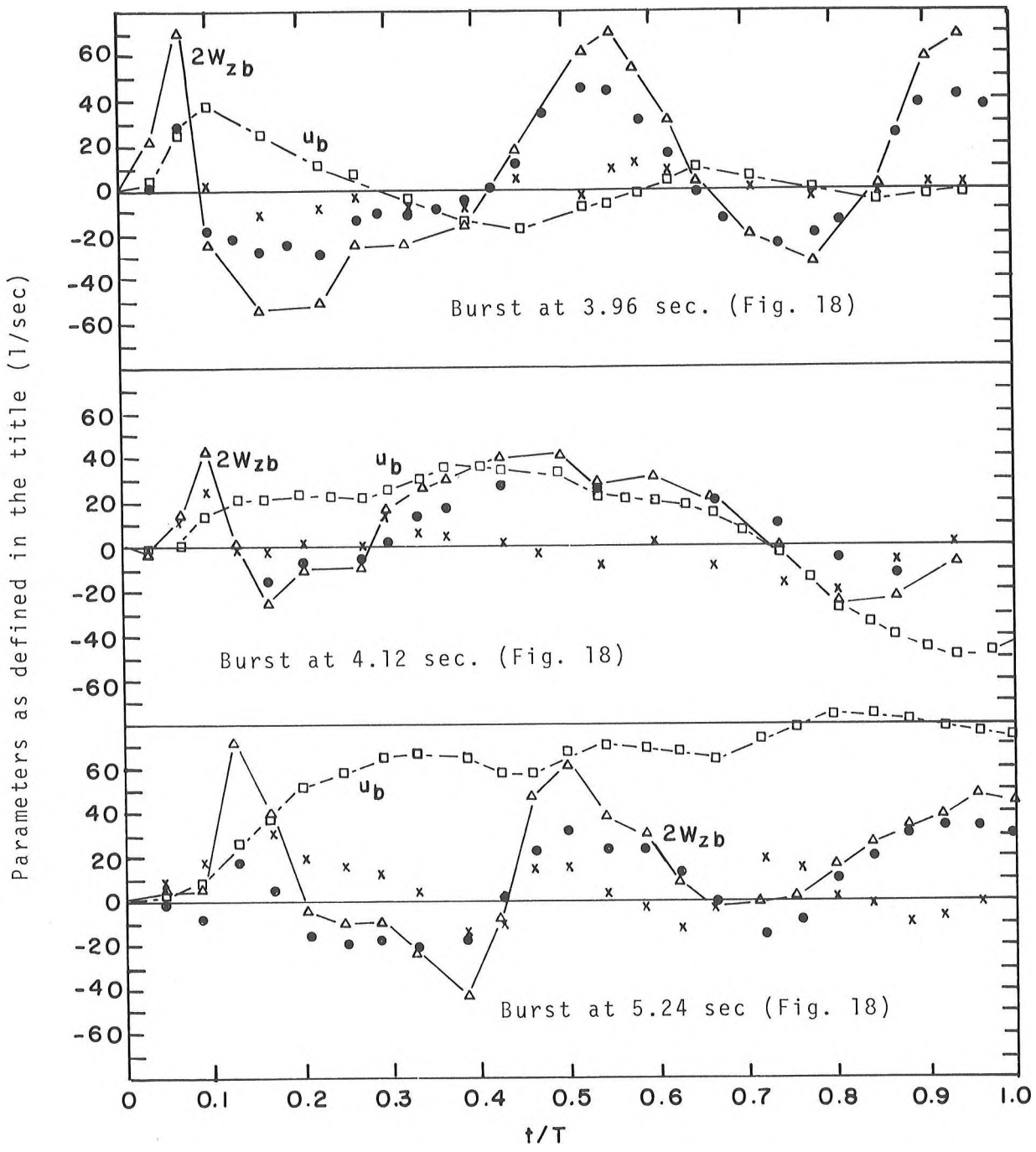

$$\square = \frac{Cx(u(t/T)-u(0))}{\bar{U}xT} = u_b, \text{ where: } C = \text{an arbitrary scaling factor and } T = \text{the burst's duration.}$$

$$\bullet = \left.\frac{\partial u}{\partial r}\right|_{t/T} - \left.\frac{\partial u}{\partial r}\right|_{0} = \left(\frac{\partial u}{\partial r}\right)_b$$

$$x = \left.\frac{\partial u}{\partial t}\right|_{t/T} - \left.\frac{\partial u}{\partial t}\right|_{0} = \left(\frac{\partial u}{\partial t}\right)_b$$

$$\triangle = \sqrt{2}\left(\frac{\partial u}{\partial r}\right)_b + \frac{1}{\bar{U}}\left(\frac{\partial u}{\partial t}\right)_b = \left(\frac{\partial u}{\partial y}\right)_b = 2x\omega_{zb}$$

Figure 14. Behavior of several variables within typical burst intervals.

development before breaking down to turbulence, the shear layer developed a kink and a second low velocity spike was seen in the u(t) trace. Contours of constant vorticity obtained during this last stage are given by Kovaszney, et al. If a pattern similar to that shown by Kovasznay, et al., perhaps less regular and more wrinkled, passed over a probe stationed at a fixed point, traces similar to Figure 14 would be the result. We did not observe an amplified oscillation before each turbulent burst. However, this is to be expected since even in the case of laminar to turbulent flow transition no selective amplification of sinusoidal oscillations is observed if there is even a small level (∿1%) of free stream turbulence. Transition is then caused directly by the random disturbances.

The negative spikes in the transition case and the relative minimums of u(t) at the beginning of bursts are probably the same since both are caused by the lifting of a patch of low speed fluid. The spikes are less distinct in the turbulent case since a natural (rather than an imposed) disturbance* is involved and since the phenomenon is superimposed on a turbulent (rather than laminar) background. The fact that the first and second vorticity peaks during each burst are of the same magnitude suggests that a wrinkled single shear layer is passing the measuring point and not discrete vortex filaments. This wrinkling may be due to a secondary instability** which would cause a weak periodicity in u(t) during burst intervals. The short-term energy spectra shown in Figure 15 support this hypothesis.

The peaks in the energy spectra taken within bursts (Figure 15) agree with the weak periodicity observed in the velocity traces of Figure 13. Although most burst spectra had peaks, the frequency of these peaks "jittered" from burst to burst. Thus, conventional ensemble averaging of the spectra of many bursts produced the smooth curve also shown on Figure 15. Since any short time spectrum may have a peak in it somewhere depending on the averaging time, it will be necessary to perform some sort of conditional averaging of many spectra before a definite periodicity can be identified. However, a "jitter" in wavelength is consistent with the two-part model of Lahey and Kline (14), which has successfully represented some of the structural features of turbulent boundary layers. This model hypothesizes that organized disturbance waves interact with background turbulence. All measurements in this and the previous section support the use of this type of two-part model to describe turbulent wall layers, rather than an 'average eddy' structure.

Summary Remarks Regarding the Intermittent Character of the Near Wall Region

Visual studies have shown that the bursting cycle always begins with the outward motion of a low speed vortex segment which forms an inflectional instantaneous velocity profile (see Kline et al. (12), Figure 19). The formation of an inflectional velocity profile is due to the addition of the excess mean vorticity of the displaced vortex segment to the mean vorticity that existed before the vortex lifted.

Bursts develop from this stage in two ways:

1) Formation and development of a transverse vortex which travels downstream developing and is finally destroyed.

2) Formation of a streamwise vortex which travels downstream increasing in both rotational speed and diameter, and is eventually destroyed. It is evident from this work that bursts sensed in this study are the eventual breakdown of these vortices to more chaotic turbulence. The results also show that this breakdown is similar to the LAST stage of the laminar-to-turbulent flow transition studies of Kovasznay, et al. (13). The FIRST stage of this transition is shown by Kline, et al. (12) to be similar to the beginning of the burst cycle.

---

* Landahl (15) has demonstrated that Tollmien-Schlichting waves of random phase and amplitude are excited in turbulent wall layers.

** The data of both Klebanoff et al. (11) and Kovasznay, et al. (13) and more recently the theoretical treatment of Landahl (15) suggest this phenomenon is the cause of the final breakdown to turbulence in the laminar-turbulent flow transition.

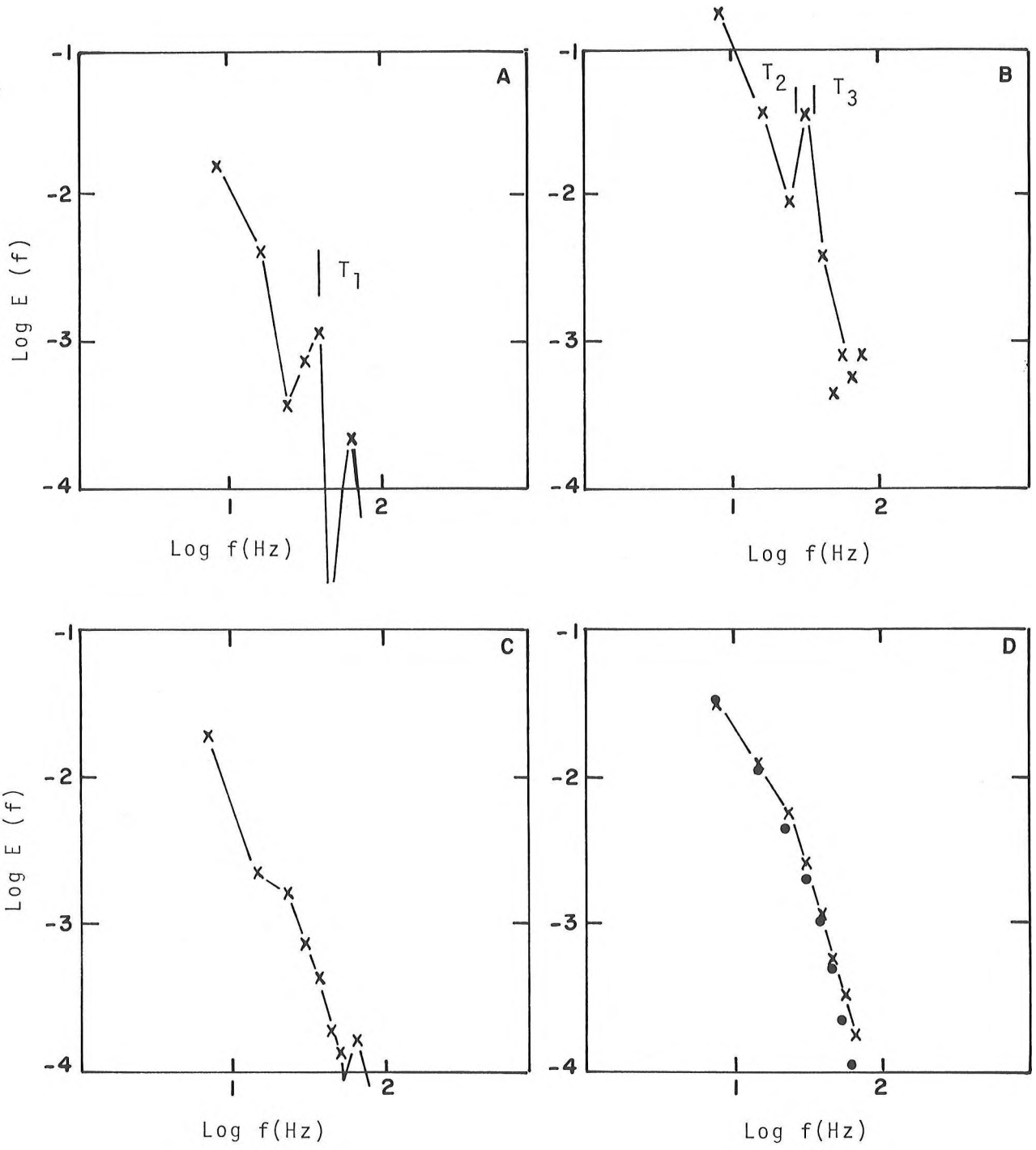

A. Burst interval from 4.13 to 4.2 sec.
B. Burst interval from 5.1 to 5.22 sec.
C. Quite interval from 4.85 to 5.1 sec.
D. x-ensemble average of 15 bursts 0-1 minute time average.

All spectra are normalized by the 1 minute average variance. The time intervals shown correspond to the intervals indicated on Fig. 14. T_1 = 0.025 sec., T_2 = 0.0375 sec., T_3 = 0.0325 sec.

Figure 15. Typical energy spectra, E(f), of u(t) taken during the active and passive intervals shown on Figure 14.

Hence it seems plausible that the intermediate stages are similar. If this is the case, the lifted vortex will continue to stretch into an elongated hairpin shape. Depending on whether the flow was marked at the head or on the arms of the hairpin this development would be seen as either (1) or (2).

After being stretched and grown for a time the vortex breaks down into more chaotic motion. The motions which result from this breakdown can evidently be characterized by a single stationary average wave model. The existence of structures which may be deterministic (the vortex filaments) in a more random background for $y^+ \lesssim 30$ may make it neither possible nor desirable to characterize this region by a single average eddy model.

CONCLUDING REMARKS

The study of turbulent pipe flow presented in the previous sections has essentially been broken into two parts. The first part studied a wave decomposition of the axial velocity fluctuation, u. This decomposition led to the use of two novel parameters to characterize the inherent organization of the flow. This "average" model was only successful for $y^+ \gtrsim 26$, possibly because of the intermittent nature of the near wall flow (which was also investigated). The wave decomposition envisages u(t) as being caused by the superposition of a field of Fourier wave components which are at an angle, $\alpha(f)$, to the wall, and moving at a speed $C_1(f)$ in the axial direction.

Difficulties were encountered in modelling the near wall region by the above "average" parameters. This was possibly due to problems caused by the intermittent long time scale periods of intense activity in the wall region. The behavior of the flow during these 'bursts' was investigated and a qualitative model of the flow structure presented.

SYMBOLS

$C_1(f)$	axial component of the phase velocity of the frequency component, f
f	frequency
$G_1(f)$	done dimensional spectrum of $u_1(t)$ (similarly for $G_2(f)$)
Q(f)	quadrature spectrum $u_1(t)$ and $u_2(t)$
R	pipe radius
Re_c	Reynolds number based on pipe radius and centerline velocity
R(f)	coherence between two signals $u_1(t)$ and $u_2(t)$
r	distance between the hot-film anemometer sensors in the special hot-film probes used in this study
t	time
$u_1(t)$	fluctuating axial velocity measured at point 1 (similarly for $u_2(t)$)
Ug	group velocity
$\overline{U}$	local mean velocity
x	axial coordinate direction
y	radial coordinate direction measured from the wall
$\alpha(f)$	inclination to the wall of the frequency component f
β	angle between the chord joining the hot-film sensors and the wall
$\theta_{12}(f)$, $\theta_{12}(\omega)$	phase shift of a wave of radial frequency ω or linear frequency f from point 1 to point 2
ω	radial frequency

REFERENCES

1. Brillouin, L., Wave Propagation and Group Velocity, Academic Press, New York, 1960.
2. Burchill, W. E., Ph.D. Thesis, Dept. Nucl. Eng., University of Illinois-Urbana, 1970.
3. Clauser, F. A., "Turbulent Boundary Layer", Adv. in Appl. Mech., 4, (1956).
4. Cooley, J. W., and Tukey, J. W., "An Algorithm for the Machine Calculation of Complex Fourier Series", Mathematics of Computation, 19, 297 (1965).
5. Favre, A. J., J. Appl. Mech., 22, 241 (1965).
6. Heidrick, T. R., Azad, R. A., and Banerjee, S., Nature (Physical Science), 234, 136 (1971).
7. Heidrick, T. R., Azad, R. A., and Banerjee, S., "Turbulence in Liquids", Ed. by Zakin, J. L., Patterson, G. K., Univ. of Missouri-Rolla, Cont. Educ. Series, 1972.

8. Heidrick, T. R., Banerjee, S., and Azad, R. S., Intern. Union Theor. Appl. Mechanics, XIII Congress, Moscow, U.S.S.R., 1972.

9. Heidrick, T. R., Ph.D. Dissertation, The University of Manitoba, 1973.

10. Kim, H. T., Kline, S. J., and Reynolds, W. C., J. Fluid Mech., 50, 133 (1971).

11. Klebanoff, P. S., Tidstrom, K. D. and Sargent, L. M., J. Fluid Mech., 12, 1 (1962).

12. Kline, S. J., Reynolds, W. C., Schraub, F. A., and Runstadler, P. W., J. Fluid Mech., 30, 741 (1967).

13. Kovasznay, L. S. G., Komoda, H., and Vasudeva, B. R., Proc. 1962 Heat Transfer and Fluid Mech. Inst., Stanford University Press, 1962.

14. Lahey, R. T., and Kline, S. J., Report MD-26, Dept. Mech. Eng., Stanford University (1971).

15. Landahl, M. T., J. Fluid Mech., 29, 441 (1967).

16. Landahl, M. T., J. Fluid Mech., 56, 775 (1972).

17. Morrison, W. R. B., Ph.D. Thesis, Dept. of Mech. Eng., Univ. of Queensland (Australia), 1969.

18. Prandtl, L., 1926 Über die ausgebildete Turbulenz. ZAMM 5, 136-139 (1925) and Proc. 2nd Intern. Congr. Appl. Mech., Zurich, 62-75; also Coll. Works, 11, 736-751, as ref. in Schlichting (21).

19. Roshko, A., NACA Tech. Note 2913, 1953.

20. Saltvold, J. S., Proc. DECUS. (Digital Equipment Users Society) Symp., Fredrickton, New Brunswick (1971).

21. Schlichting, H., Boundary Layer Theory, McGraw-Hill, 1968.

22. Stegen, G. R., and Van Atta, C. W., J. Fluid Mech., 42, 689 (1970).

23. Sternberg, J., Physics of Fluid Suppl., S146, 1967.

24. Townsend, A. A., The Structure of Turbulent Shear Flow, Cambridge Univ. Press, 1956.

25. Townsend, A. A., Boundary Layer Research Symposium, Int. Union of Theo. and Appl. Phy., Springer, Berlin, as ref. by Morrison (17).

26. Townsend, A. A., J. Fluid Mech., 11, 97 (1961).

27. von Karman, Th., NACA TM 611, 1931; also Coll. Works, 11, 337-346, as referenced by Schlichting (21).